THE ASTROPHYSICAL JOURNAL, 402:230–237, 1993 January 1

AMMONIA IN THE W3(OH) REGION

T. L. WILSON,[1] R. A. GAUME,[2] AND K. J. JOHNSTON[2]
Received 1992 April 10; accepted 1992 July 13

ABSTRACT

Maps in the $(J, K) = (1, 1)$ and (2, 2) inversion lines of NH_3 made with 3″ angular resolution (=0.03 pc at 2.2 kpc) show the presence of optically thick unresolved emission 5.″2 east of the compact H II region W3(OH). The position agrees with previous HCN results. This clump is about 0.″8 west of the center of the group of H_2O masers; the virial mass is 18 $M_\odot$. From the virial mass and estimated radius, 0.006 pc, the average density is 4×10^8 cm^{-3}. From the peak H_2 column density, 10^{25} cm^{-2}, and the NH_3 column density, 10^{17} cm^{-2}, the NH_3/H_2 ratio is 10^{-8}.

As found previously, there is prominent absorption toward the high surface brightness, compact H II region W3(OH). However, toward W3(OH), there is no emission counterpart to the NH_3 absorption. There are weak, extended emission features more than 15″ SE and SW of W3(OH). This emission is not found to the north of W3(OH). This asymmetrically distributed emission would seem to provide an argument against a toroidal belt of molecular gas surrounding W3(OH).

The largest scale feature is a remarkable, 1.′5 long, less than 20″ wide filament which extends from N of the H II region–H_2O maser complex to the NE. Within this filament there are at least five maxima. The T_k in this region is of order 20–30 K, and the FWHP line width is less than 2.4 km s^{-1}. From virial estimates, the molecular mass in our map is less than 200 $M_\odot$.

Subject headings: ISM: individual (W3) — ISM: molecules — radio lines: ISM

1. INTRODUCTION

The W3(OH) region is an active site of star formation located 2.2 kpc from the Sun (see, e.g., Dickel & Goss 1987). This area is optically obscured and consists of a 2″ (0.02 pc) diameter shell-like H II region W3(OH), where the OH masers are found (Dreher & Welch 1981). A cluster of H_2O masers is located 7″ to the east of the H II region (see, e.g., Turner & Welch 1984).

In the centimeter wavelength range, NH_3 molecules in the foreground cloud absorb continuum free-free radiation from the compact H II region through inversion transitions. In the NH_3 inversion lines, W3(OH) has been studied with 0.″2 resolution by Guilloteau, Stier, & Downes (1983) and Reid, Myers, & Bieging (1987). These maps show that this gas covers a total area of about 2″ in declination by 1″ in R.A., and is located in the western part of the source. Maps of the 6 and 2 cm lines of H_2CO with 0.″5 resolution (Dickel & Goss 1987) show that lower density gas is located toward the eastern part of W3(OH). Since the NH_3 usually traces denser gas, the H_2CO and NH_3 results are in good agreement. The OH (Norris, Booth, & Diamond 1982) and methanol (Menten et al. 1988) masers are located toward the western part of W3(OH), as is the methanol absorption, while hot, thermally excited OH seems to be present over a larger region (Wilson, Johnston, & Mauersberger 1991). The continuum emission is elongated SW-NE, with a lower surface brightness extension to the NE (Guilloteau et al. 1983; Guilloteau, Baudry, & Walmsley 1985). The ionized gas is extended in a direction perpendicular to the direction of the denser molecular gas, as traced by the NH_3 and maser centers. Guilloteau et al. (1983) interpreted these reults in terms of a torus of molecular material surrounding the compact H II region, allowing expansion to the NE. Single-telescope multiline studies of NH_3 showed that the kinetic temperature of the absorption-line region is 95 K (Wilson, Mauersberger, & Henkel 1988). The radial velocity of the absorption lines from the densest gas is −44.7 km s^{-1}, and the FWHP line width is 1.5 km s^{-1}.

Turner & Welch (1984) have published the only very high angular resolution study (beam about 1.″2) of the H_2O maser center in quasi-thermally excited molecular lines. This showed that the size of the HCN emission region is less than 1″ and that the clump is centered about 1″ west of the cluster of H_2O masers. The peak HCN line brightness temperature is more than 100 K. Turner & Welch argued that the molecular clump near the H_2O masers cannot be heated by W3(OH) and concluded that the heating must be internal. Single-telescope, 40″ resolution, multiline studies of NH_3 showed an increase in the kinetic temperature with energy above ground (Mauersberger et al. 1988), consistent with a centrally heated region.

In contrast to the two compact sources, only a few studies have been made of the more extended gas. The 10″ resolution continuum map made by Harten (1976) showed evidence for four weaker H II regions, in addition to W3(OH). A 10″ resolution map of the (1, 1) and (2, 2) inversion lines of NH_3 by Keto, Ho, & Reid (1987) showed emission centered close to the HCN peak, and also weaker emission to the west of W3(OH). These authors commented that there seemed to be no emission toward W3(OH) itself, but discussed the possibility that this emission might be hidden in the deep absorption from the foreground cloud. These results were limited by noise to only the brightest maxima. From the 12″ maps of Wilson et al. (1991), the V_{LSR} of the molecular line emission decreases from −46 to −48 km s^{-1}, between the position of W3(OH) and the H_2O maser center, and both are located to the north of the densest molecular cloud. Studies in the (1, 1), (2, 2), and (3, 3) inversion lines of NH_3 made with a 40″ beam by Wilson, Bieging, & Downes (1978) and Zeng et al. (1984) showed that

[1] Max-Planck-Institut für Radioastronomie, Auf dem Hügel 69, W53 Bonn, Germany.
[2] Center for Advanced Space Sensing, Naval Research Laboratory, 4555 Overlook Avenue, Washington, DC 20375-5000.

the NH_3–emitting region has a size of about 1′, and that the kinetic temperature of this gas is about 30 K. In order to investigate the lower surface brightness molecular gas in more detail, we have made spectral line maps with the D-configuration of the VLA.

2. OBSERVATIONS

The observations were made on 1991 April 26, using all 27 antennas of the VLA,[3] in the D-configuration. Two analyzing bands, each of width 6.25 MHz, were centered on the $(J, K) = (1, 1)$ and (2, 2) lines, with assumed rest frequencies of 23694.496 and 23722.631 MHz. Each band was divided into 64 contiguous channels. The data were Hanning smoothed on-line to obtain a velocity resolution of 1.2 km s^{-1}. Channel 32 of each band was centered at $V_{LSR} = -46.0$ km s^{-1}. A full 12 hour synthesis was made by alternately observing W3(OH) in each transition, at R.A. = $02^h23^m16^s.9$, decl. = +61°38′57″.4 (B1950.0), for 13 minutes, and then the phase calibrator, 0224+671, for 4 minutes at each transition. The flux density scale was calibrated by observations of 3C 286, which was assumed to have a flux density of 2.4 Jy at 1.3 cm. Bandpass calibration was accomplished through observations of 3C 84. The data were processed using the standard AIPS package of NRAO operating on NRL computer systems. Self-calibration was performed on the higher signal-to-noise continuum channel. The self-calibration gain adjustments were applied to all spectral line channels. The agreement of the position of the continuum peak of the W3(OH) H II region in the original and self-calibrated maps was excellent, so no positional adjustments of the self-calibrated maps were made. After self-calibration the UV data were transformed in three different ways to emphasize features at different spatial scales. Uniform weighting of the UV data resulted in a synthesized beam size of 2″.2 × 2″.1 with a position angle of 85°. Natural weighting of the UV data provided greater sensitivity at the cost of slightly degraded resolution (beam size 4″.0 × 3″.6, p.a. 82°). To improve sensitivity to extended structures, natural weighting with a 20 kλ Gaussian taper was applied to the UV data resulting in a beam size of 9″.2 × 8″.4, p.a. 82°. The natural weighted and tapered data were transformed into images with a pixel size of 1″. The uniform weighted data were transformed into images with a pixel size of 0″.5. After transformation of the data into the image plane, a continuum image was constructed from a total of 14 channels free of line emission, from both ends of the bandpass. The continuum image was subtracted from the data to produce images that contained only line emission, which were then restored with a beam deconvolution algorithm.

Additional observations of W3(OH) in the (1, 1) and (2, 2) inversion lines were carried out with the 100 m telescope. The beam size is 40″ at the line frequency. The receiver noise temperature, including the atmosphere, was 100 K. The autocorrelation spectrometer was used as two 512 channel receivers. The spectra were twice smoothed so that the final velocity resolution was 0.6 km s^{-1}. The data were taken using position switching, with one reference spectrum for 3-4 on source spectra. The calibration procedures followed the method outlined in Wilson & Mauersberger (1990).

[3] The VLA is a facility of the National Radio Astronomy Observatory operated by Associated Universities, Inc., under a cooperative agreement with the National Science Foundation.

3. RESULTS

Figure 1 is a contour map of an image made from integrating four channel maps in the velocity range −46.0 to −49.7 km s^{-1}. The resolution of this map is 9″.2 × 8″.4, p.a. 82°. This shows the larger scale distribution of the emission-line gas at these radial velocities. A cross marks the position of the H II region W3(OH). The prominent absorption against W3(OH) is narrow and has V_{LSR} of about −44.5 km s^{-1}; hence it is not present in this map. There is unresolved emission near the H_2O center. This emission is 5″.8 east of W3(OH) and 0″.8 west of the center of the cluster of H_2O masers. The most prominent feature is the extended filamentary emission. This feature begins slightly NE of the H_2O maser center, extends for about 40″ to the east, and then bends to the NE. The total extent is over 1′.5. Within the extended emission are at least five maxima. There are also extended features southeast and southwest of W3(OH).

We present a series of four velocity channel maps of the (1, 1) inversion line in Figure 2. These have been produced from the natural weighted, untapered data with an angular resolution of 4″.0 × 3″.6. There is deep absorption toward W3(OH) in the velocity channel at −44.8 km s^{-1}. This is absent at V_{LSR} more negative than −47.2 km s^{-1}. At −46 km s^{-1} there is extended, lower brightness emission to the SW and S of W3(OH). At −47.2 km s^{-1} there is a fairly bright patch of emission at an offset of (+59″, +18″) from W3(OH).

In the next velocity channel, −48.5 km s^{-1}, this feature has disappeared, and the long tenuous filament of emission, prominent in Figure 1, is seen. Some of this emission is present in the next velocity channel, at −49.7 km s^{-1} (not shown). To the east of the absorption, there is a compact source of emission,

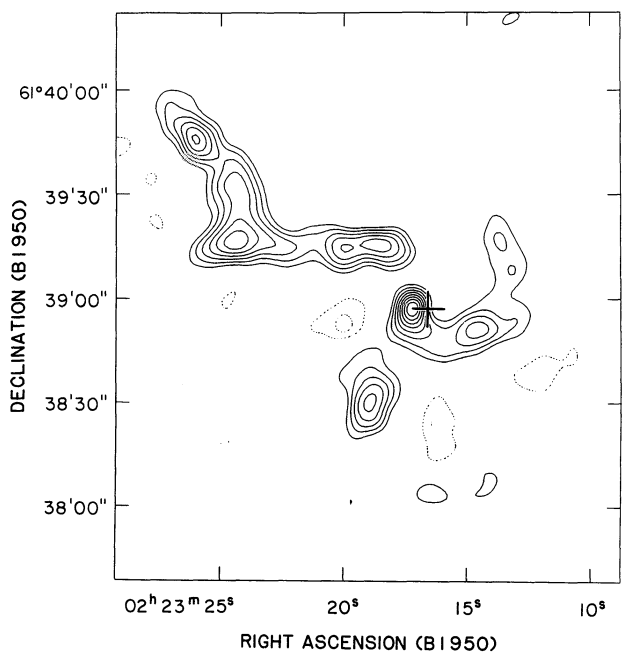

FIG. 1.—Contour map of the $(J, K) = (1, 1)$ inversion line of NH_3, for the sum of four channels covering the V_{LSR} range from −46.0 to −49.7 km s^{-1}. The contour levels are −30%, −20%, 20%, 30%, 40% ... of the peak flux density beam^{-1} which is 0.25 Jy km s^{-1} beam^{-1}. This map was produced using a taper of 20 kλ and natural weighting of the UV data; the resulting angular resolution is 9″.2 × 8″.4, p.a. 82°. These data are not corrected for the taper in the primary beam of the VLA telescopes.

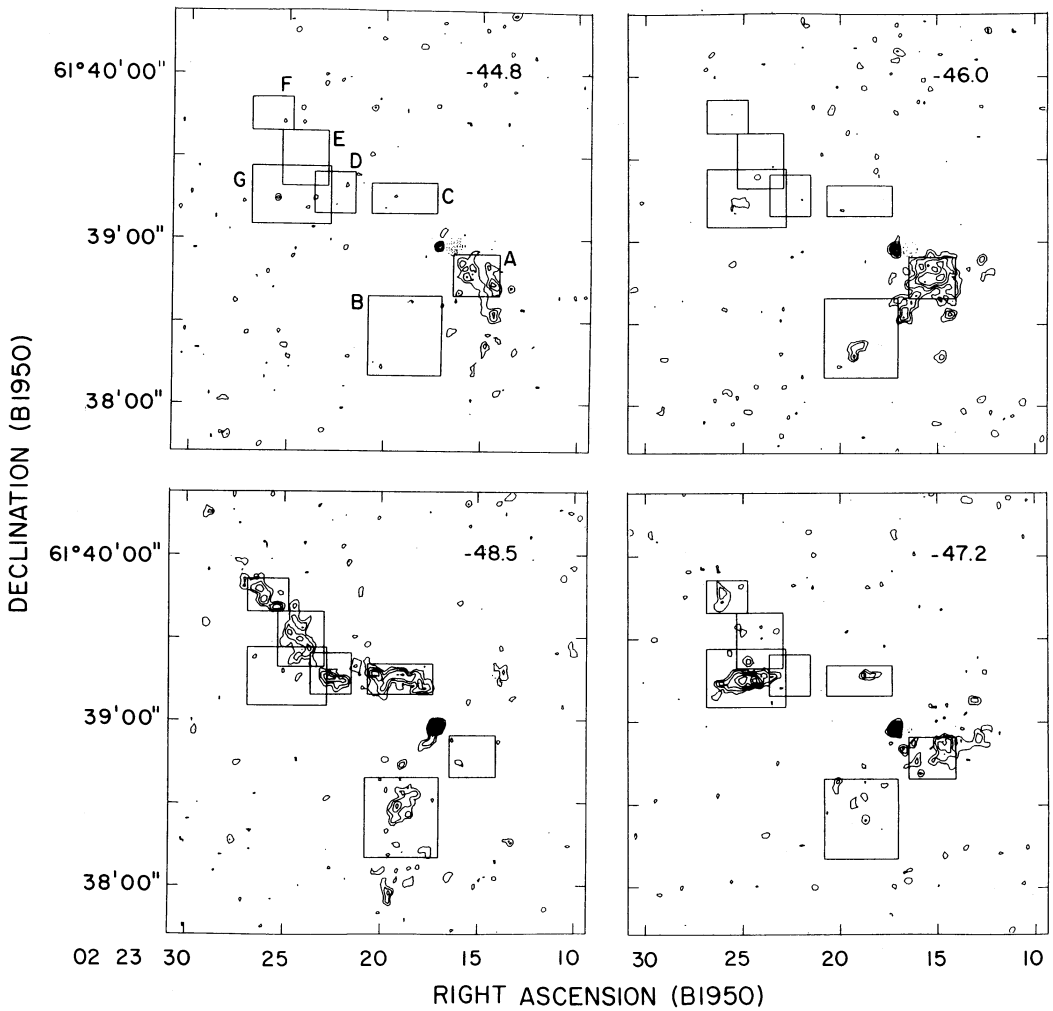

FIG. 2.—Collection of four velocity channel maps, for the $(J, K) = (1, 1)$ inversion transition of NH_3. These were produced from 4″ × 3.″6, p.a. 82°, natural weighted data. The panels are arranged in order of increasing radial velocity. The V_{LSR} are given in the upper right of each panel. The spacings of the contours are $-90, -70, \ldots, -10, 2, 3, \ldots$ 13 times 7.5 mJy beam^{-1}. The peak is equivalent to 20 K. The boxes enclosing the regions mark the boundaries where spectra were formed by integrating over the regions shown. These spectra are shown in Fig. 3. The cross marks the location of the compact H II region W3(OH). These data are not corrected for primary beam taper.

peaking in the -47.2 km s^{-1} channel, close to the H_2O maser cluster.

In Figure 3 we show spectra of the (1, 1) and (2, 2) inversion lines produced by summing over rectangular regions shown in Figure 2. The spectra have been analyzed following the methods outlined in the Appendix; these have been reduced using a by-eye analysis, and the results are given in Table 1. The NH_3 optical depths of the extended sources are less than unity. In contrast, those of the absorption lines are at least 1.5–2. For the H_2O center, the optical depths are 2–5. The NH_3 data provide estimates of T_k, virial masses, H_2 densities (from the source size and virial mass), and the abundance ratio (NH_3/H_2). Since only the (1, 1) and (2, 2) inversion lines have been measured, our data are most sensitive to gas cooler than 100 K.

In Figure 4 we show NH_3 profiles taken with the 100 m telescope in the (1, 1) inversion line on an R.A.–decl. grid. The 100 m data show that the 1.′5 long filament extending to the NE is clearly present in single-dish maps. Although the emission extends to the edge of our map, additional unpublished data show that it does not extend much further than the boundary of the VLA map. A comparison between the VLA and 100 m intensities shows that at an offset of (40″, 40″) from W3(OH), all of the flux density in the filament has been recorded by the VLA. At larger offsets, the corrections for the taper of the primary beam of the individual VLA antennas are too large to give an accurate comparison. Toward W3(OH) and the H_2O maser center, the VLA records less than 60% of the single-dish ammonia line intensity. The 100 m data shows clearly that some of the clouds measured in NH_3 are south of W3(OH) and the H_2O center. There is NH_3 to the west of W3(OH), but much of this is not found in the VLA maps. Presumably this is cooler gas which has a low brightness temperature.

We show our higher angular resolution, uniform weighted map in Figure 5. Superposed on this are positions of the H_2O maser centers and the H II region found by Guilloteau et al. (1985). The ammonia absorption-line region is unresolved by our beam. We have taken the Gaussian FWHP of the absorption-line region as 0.″7, one-half of the total extent of the absorption determined from the higher resolution VLA maps of Guilloteau et al. (1983) and Reid et al. (1987).

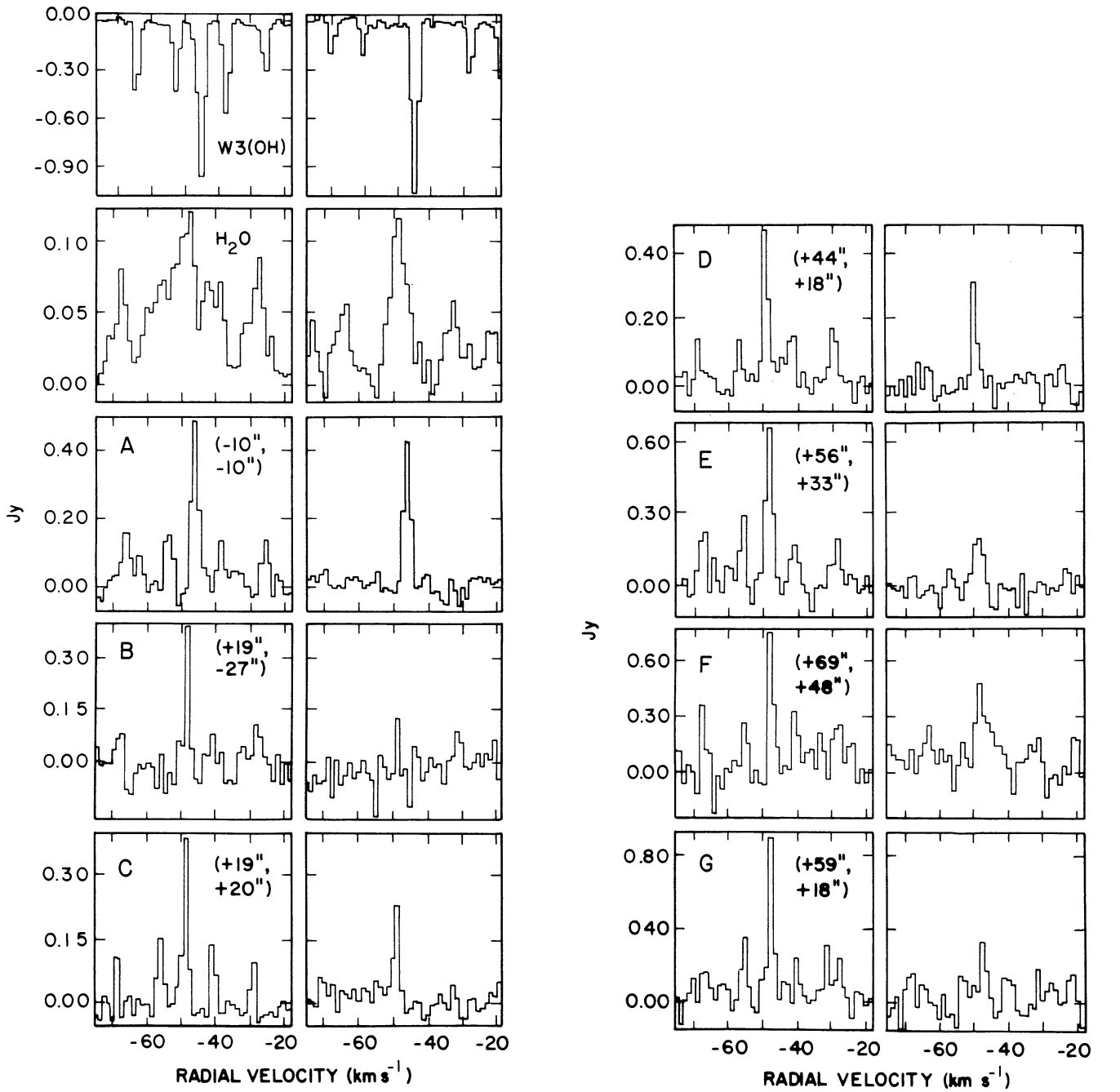

FIG. 3.—Collection of spectra for the (1, 1) and (2, 2) inversion transitions. The spectra have been corrected for primary beam taper. The intensity scale is in Jy, summed over boxed regions shown in Fig. 2. The cloud names and offsets serve to identify the sources in Table 1. In the case of small optical depth, the ratio of satellite hyperfine (HF) components is 0.22 for the inner and 0.28 for the outer groups of satellite HF components; in the case of the (2, 2) inversion line, the satellites are 0.06 of the main group of HF components. The NH_3 emission from Clouds A to G are optically thin, while the inversion lines from W3(OH) and the H_2O source are optically thick.

The molecular regions closest to W3(OH) and the H_2O center have the highest rotational (and thus kinetic) temperatures. The next warmest region is $(-10'', -10'')$ from W3(OH); all other regions are significantly colder. However, all of these T_{ROT} values are much warmer than 10 K, the kinetic temperature of dark dust clouds containing no high-mass stars. The simplest assumption would be that O-B stars close to these regions provide the heat input needed.

The width of the absorption line is comparable to our velocity resolution, and we have taken the value of 1.5 km s^{-1} from Mauersberger et al. (1988). The width of the line from the H_2O region is the largest measured in this region. If caused by the response to gravity (and not by outflowing gas; see Alcolea et al. 1992), the mass and density of this region must be extremely large. In contrast, the line widths from the maxima in the filament are fairly narrow.

The FWHP angular sizes of maxima away from W3(OH) and the H_2O center were obtained from the natural weighted

TABLE 1

CLOUD PARAMETERS

Name (1)	Offset from W3(OH)[a] (α, δ) (2)	Radial Velocity V_{LSR} (km s^{-1}) (3)	FWHP $\Delta V_{1/2}$ (km s^{-1}) (4)	FWHP geometric Mean Size (10^{-2} pc) (5)	Virial Mass ($M_\odot$) (6)	$n(H_2)$ (cm^{-3}) (7)	T_{ROT} (K) (8)	$N(H_2)$ (10^{23}) (9)	$X(NH_3)$ (10^{-8}) (10)
W3(OH)	(0, 0)	−44.6	1.5[b]	1.0[c]	6	3×10^7	95[d]	9[f]	6
W3(H_2O)	(+5.″2, +0.″5)	−49.0	4.2	1.2[g]	18	4×10^8	40[e]	300[f]	2
(A)	(−10, −10)	−46.0	2.4	18	80	6×10^5	30	3	0.1
(B)	(+19, −27)	−48.5	<1.2	10	<5	$<2 \times 10^5$	17	<0.6	>0.6
(C)	(+19, +20)	−48.5	<1.2	<7	<5	$<2 \times 10^5$	22	<0.4	~8
(D)	(+44, +18)	−48.5	2.4	8	50	4×10^6	25	10	0.1
(E)	(+56, +33)	−48.5	2.4	16	15	9×10^5	17	4	0.1
(F)	(+69, +48)	−48.5	<1.2	14	<5	9×10^4	22	<0.4	>1
(G)	(+59, +18)	−47.2	<1.2	12	<5	$<1 \times 10^5$	18	<0.4	>1

[a] At $\alpha = 02^h23^m16^s.4$ $\delta = +61°38'57''.4$ (B1950).
[b] Line width from Mauersberger et al. 1988; other line widths are *not* deconvolved from 1.2 km s^{-1} channel width.
[c] From the size of the NH_3 absorption-line maps of Guilloteau et al. 1983 and Reid et al. 1987.
[d] Taken from Mauersberger et al. 1988.
[e] Assumed T_{ex} for the (2, 2) inversion line (see Mauersberger et al. 1988).
[f] Deconvolved values for peak; all others are beam averaged.
[g] Size obtained from excitation calculation (see text).

channel maps in Figure 2. The masses of the regions are obtained from an application of the virial theorem (see Appendix). The average H_2 densities have been obtained from the virial masses, assuming a uniform density, spherical geometry. We collect the source parameters in Table 1.

For extended emission regions, the (NH_3/H_2) ratios, X, have been calculated using the prescription in the Appendix. The X-values are comparable to those found for moderately dense dust clouds. The NH_3 abundances of the absorption-line and H_2O region have been obtained with additional information from multilevel observations (Mauersberger et al. 1988). The value for the absorption-line region has been discussed extensively (see, e.g., Mauersberger et al. 1988 for references).

4. DISCUSSION

4.1. *Relation of the H II Region with Nearby Extended Clouds*

Cloud A (see Table 1) is 15″ SW of the compact H II region. In the $J = 5$–4 and $J = 3$–2 lines of $C^{34}S$ in the 12″ maps of Wilson et al. (1991), this cloud was found to be an unresolved source, that is, the FWHP size is less than 6″. On the basis of the $C^{34}S$ line intensity ratio, the H_2 density in this cloud is

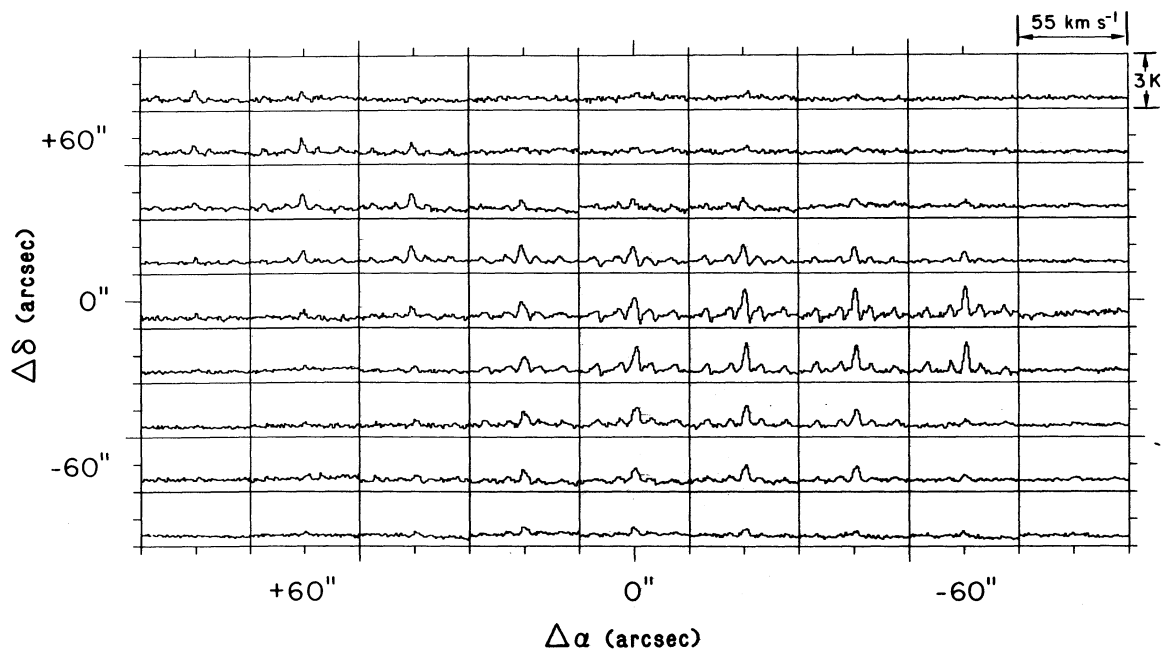

FIG. 4.—Plot of (1, 1) NH_3 spectra taken with the 100 m telescope (angular resolution 40″). The offsets are with respect to W3(OH), which is centered at R.A. = $02^h23^m16^s.5$, decl. = +61°38′57″.0 (1950.0). The spectra have been smoothed twice, so that the velocity resolution is 0.6 km s^{-1}. The intensities are on a main beam brightness temperature scale, where 1 K = 0.8 Jy beam^{-1}. The intensity scale is −0.6 K to 2.4 K T_{mb}; the velocity scale from −75 to −20 km s^{-1}.

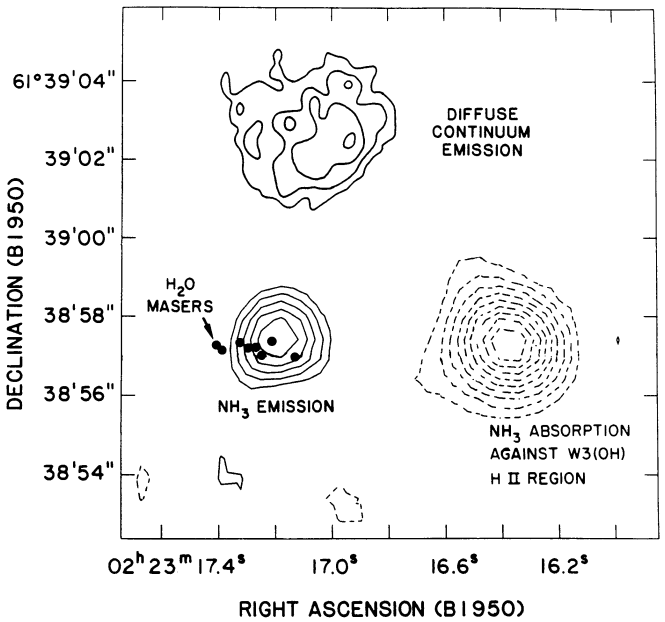

FIG. 5.—Map of the NH_3 contours toward W3(OH) and the H_2O center (*lower part*) and a diffuse continuum source (from Guilloteau et al. 1985) (*upper part*). The positions of H_2O masers (taken from Turner & Welch 1984) are shown as filled circles. This map is the sum of channels between $V_{LSR} - 43.5$ to -49.7 km s^{-1}. The contours for the absorption line range from -1.98 Jy km s^{-1} beam^{-1} to -0.2 Jy km s^{-1} beam^{-1}, in steps of 10%. For the emission line, the contours are 0.198 Jy km s^{-1} beam^{-1} to a peak value of 0.395 Jy km s^{-1} beam^{-1} in equal steps.

about 10^7 cm^{-3}. From our estimate in Table 1, the H_2 density is 10^6 cm^{-3}. The larger size and lower H_2 density is consistent with a core-halo cloud structure. The higher T_k indicates that the close position of W3(OH) and cloud A is not a coincidence, but rather there is a direct connection. From the map at -46 km s^{-1}, in Figure 2, the H II region is at the NE boundary of cloud A. There is *no* NH_3 emission toward W3(OH) itself, or 3″ to the north. It would be difficult, on the basis of these results, to find evidence for the symmetric torus of molecular gas predicted by the model of Guilloteau et al. (1983). More quantitative estimates are possible: Toward the H II region, the beam-averaged column density is 5×10^{16} cm^{-2} in metastable levels. If there were a symmetric torus of molecular gas, ammonia in the back side of the torus would give rise to emission. A comparison of the absorption-line flux density from single-dish and VLA spectra might allow an estimate of the amount of emission toward the H II region; however, this is very uncertain, since in the single-dish beam the absorption is mixed with emission from the H_2O maser region and cloud A, also. The best limit for emission from a symmetric torus structure around W3(OH) can be set from the absence of emission to the 1 K (=7.5 mJy beam^{-1}) level one beamwidth to the north of W3(OH). If such NH_3 emission were optically thin, with $\Delta V_{1/2} = 1.5$ km s^{-1} and a rotational temperature of 20–50 K, the equivalent column density is 10^{14} cm^{-2} from W3(OH) in the metastable inversion levels, averaged over our beam. To the SW of W3(OH), at the peak of cloud A, 14″ from W3(OH), there is 8 times this column density averaged over our beam. To the north there is at most an NH_3 column density of less than 10^{14} cm^{-2}. Thus, there must be an asymmetry in the NH_3 distribution around W3(OH), since toward the H II region, the beam-averaged column density is more than 30 times larger. Unless the material immediately north and south have larger optical depths, or very small beam filling factors, portions of the molecular toroid to the sides of W3(OH) are not present in our maps.

The proper motions of the OH masers in the foreground cloud show expansion (Bloemhof, Reid, & Moran 1992). The V_{LSR} of the cloud absorbing W3(OH) is -44.7 km s^{-1}. In the western part of the H II region, there is an ultra high density ionized clump with $V_{LSR} = -41.5$ km s^{-1} (Wilson et al. 1991). Thus, the V_{LSR} of the foreground cloud of W3(OH) are consistent with the proper motions of OH masers. Bloemhof et al. (1992) suggest that W3(OH) is a cometary H II region, moving from NE to SW, into cloud A. If this were so, the exciting star of W3(OH) was formed in the NE, near the extended H II region shown in Figure 5, and the lower density NH_3 filament. These regions have much lower densities than cloud A. If W3(OH) has not dispersed the cloud where it was born, it must have been produced in a lower density region. This is surprising, since it is thought that O-B stars should be formed in the densest molecular clouds.

4.2. *The H_2O Maser Region and Nearby NH_3 Clouds*

The H_2O clump is at the northern edge of the extended molecular cloud B, at -48.5 km s^{-1} (see Fig. 2). On the basis of the VLA data, there is only a low T_k and narrow line width for cloud B, indicating a small mass. Thus, the H_2O clump is *the* densest molecular gas at -48.5 km s^{-1}, and cloud B appears to be a low-mass, low-density cloudlet. These NH_3 results are in some disagreement with the $C^{34}S$ data of Wilson et al. (1991), which shows an unresolved cloud to the south of the H_2O maser center with a density of 10^7 cm^{-3}. However, the NH_3 data reinforce the idea that the star (or stars) in the H_2O center is young, since it is still embedded in the highest density cloud, its birthplace.

The NH_3 source near the H_2O masers is also unresolved. From an analysis of 16 NH_3 inversion lines, Mauersberger et al. (1988) found evidence for a hot core, cold halo structure. Following Mauersberger et al. (1988), we assume that the true line brightness temperature of the optically thick (2, 2) line is 40 K. From the peak line temperature, the FWHP Gaussian size is 1.″2. Wilson et al. (1991) assumed a true brightness temperature of 100 K giving a size of 0.″8. These sizes are significantly larger than the size estimated by Turner & Welch (1984) from HCN. However, the HCN may be present only in the inner part of this cloud.

Toward the H_2O masers the NH_3 line widths predict an H_2 column density of 10^{25} cm^{-2}. When diluted in a 12″ beam, this source would have a dust continuum intensity of 1.25 Jy beam^{-1} (see eq. [B1] of Wilson et al. 1991). Wink, Mezger, & Zylka (1988) find 6 Jy from dust emission which is unresolved in their 12″ beam. Thus, the column density we deduce is consistent with the data.

Surprisingly, the X-value (see Table 1) for the most extraordinary region, the H_2O maser clump, is small compared to very young, hot, and dense regions such as the Orion hot core region (see, e.g., Migenes et al. 1989 and references therein). It is thought that the high value of X in Orion KL is caused by very recent evaporation from grains. That X is lower in the H_2O maser region may indicate that this is in a more advanced stage of evolution than the Orion hot core. For the absorption-line region, the X-value is only slightly larger than in the H_2O maser region.

The hydrogen column density for the H_2O region is extraordinary by any standards. Only the largest values estimated for

the Sgr B2 regions or for the Orion hot core are comparable. Our value is 30 times that reported by Turner & Welch (1984), who used an assumed (HCN/H_2) ratio to obtain the H_2 column density. The larger HCN line width reported by Turner & Welch (1984), and the H_2O maser proper motions found by Alcolea et al. (1992), may indicate that the NH_3 line widths are affected by an outflow. If so, the masses, H_2 densities and column densities might be too large. All estimates for this source must be considered uncertain, but this source does have a very large density and column density of H_2.

4.3. *The Filamentary Structure*

The filamentary structures to the N and E of the compact regions are listed in Table 1 as the five maxima labeled C–G. These have line widths and T_k values which vary in a systematic way with distance from the H_2O center or W3(OH). These values indicate warm, fairly turbulent regions, not at all like dark dust clouds, but with a line width smaller than that found for the very compact H_2O region. For these sources, the H_2 column densities exceed 6×10^{22} cm^{-2}, similar to the Orion ridge. In Figure 5 of Wilson et al. (1991), there are signs of the filament in the $J = 2$–1 line emission of $C^{18}O$, but this emission is also present in other parts of the map, at a lower level. In the $C^{34}S$, the region mapped is too small to determine any trends. It would appear that the density is certainly greater than 3×10^4 cm^{-3}, from the presence of NH_3 metastable inversion lines. The densities obtained from virial masses are probably upper limits. At present, more definite estimates are not possible.

The remarkable shape of the NH_3 filament requires us to attempt some explanation. First, this could be an outflow which is highly collimated, and perpendicular to the line of sight. Second, the long filamentary shape is similar to a plasma pinch; this suggests a connection with magnetic fields. Third, we may be observing a small portion of the molecular gas which is warmer and denser than average; this might be heated and compressed by a collection of nearby low surface brightness H II regions. Fourth, it might be molecular material compressed by a shock wave.

Any of these explanations requires very special circumstances, since the line widths are narrow. The first explanation would require that the outflowing material moves at right angles to the line of sight, being deflected between clouds D and E without being dispersed and without additional line broadening. This seems so special that we reject it. The second explanation requires that the magnetic field dominates the dynamics. We can estimate the strength of the field required by setting the magnetic energy density equal to the turbulent energy. Using the line width 2.4 km s^{-1}, and an assumed density of 10^6 cm^{-3}, the field must have a strength of 0.7 mG.

The third explanation requires that a series of H II regions are formed parallel to the filament. The results reported by Harten (1976) show a number of low-brightness H II regions in other locations close to W3(OH). This might be interpreted as support for this notion, since low-brightness H II regions are common in this region. One found by Guilloteau et al. (1985) is shown in Figure 5. If a series of such H II regions were formed, these might be located close to the NH_3 filament, compressing and heating it. Even if heating and compression by nearby H II regions are the cause of the filament, one must explain the placement of these sources. This might be related to star formation induced by a shock wave, perhaps from O-B stars in the W3 region. This H II complex, is about 12′ (=7.7 pc) to the NW. The progression of star formation would be from W to E.

Another scheme has been favored by Lada et al. (1978). In this picture, the W4/5 region has formed first, and the shock front preceding the ionization front has led to the formation of both W3 and W3(OH). To us, it seems surprising that a shock moving from E to W would give rise to the more westerly, but also more developed W3 region, and also to the more easterly, but very much more compact (and hence presumably younger) W3(OH) region and associated molecular cloud. Of course, the formation of W3(OH) may have been delayed by some process. About 10^{44} ergs is required to explain the turbulent energy in the line widths we measure. This requirement is met by the mechanical energy of an O-star cluster, radiated in the angle subtended by the filament and W3(OH), if the energy can be accumulated in a region over a period of a few thousand years. Thus, energetics would not be a problem. But why W3(OH)? One could envisage that this is just one of many high-density, compact regions. Perhaps it is more advanced, and we have found this source because of the OH maser line emission. There might be other low-density clouds. Thus, our results might indicate that the star formation in W3(OH) could be caused by the O-B star clusters in W3/4/5, if a number of conditions are met. There might be a number of other such regions near W3 at an earlier stage of development.

5. CONCLUSIONS

High-sensitivity, 3″ angular resolution maps in the (J, K) = (1, 1) and (2, 2) inversion lines of NH_3 over a 2′ region centered on W3(OH) allow a number of conclusions about the more extended, denser molecular gas in the region where OH, methanol, and H_2O masers are found. First, one beam north of the compact H II region W3(OH), there is no emission. We can set a beam-averaged upper limit of 10^{14} cm^{-2} for this gas. One beam south of W3(OH), the column density is 2×10^{14} cm^{-2}. These values are 1/30 of that seen in absorption. This lack of molecular emission indicates that the model involving a symmetrical toroid of molecular gas around W3(OH) requires some revision. The symmetric elliptical shape of the H II region cannot be explained in a simple model involving champagne flow since molecular clouds are found only to the south. Toward the H_2O masers, there is an unresolved center of optically thick NH_3 emission. Excitation arguments indicate that the radius is 0.04 pc. Applying the virial theorem to the line width, one finds a mass of 18 $M_\odot$, and an average density of 10^9 cm^{-3}. There is a 2′ long, less than 20″ wide emission feature NE of the W3(OH) and H_2O centers. This may be related to shock fronts caused by star formation in the W3 region or nearby H II regions, but not by an outflow.

We thank C. Lemme, S. Huettemeister, and G Dahmen for help with taking the data shown in Figure 4. We also thank Hoang-An Nguyen and Han Park for assistance in reducing the VLA data, and the referee for providing useful comments. This work was supported in part by the Max-Planck-Forschungspreis, administered by the Alexander-von-Humboldt-Stiftung.

APPENDIX

The virial mass of a uniform density, spherical region is given by the relation (see Wilson & Mauersberger 1990 and references therein)

$$M_v = 250R(\mathrm{pc})[\Delta V_{1/2}(\mathrm{km\ s^{-1}})]^2 ,$$

where R is the radius of the region in pc, and $\Delta V_{1/2}$ is the FWHP line width in km s^{-1}. The average H_2 density in such a region is given by the relation

$$n(\mathrm{H_2}) = \frac{4.9M_v}{[R(\mathrm{pc})]^3} .$$

The populations of metastable inversion levels of NH_3 are exchanged almost exclusively by collisions. Thus the ratios of populations of the metastable levels are directly related to the kinetic temperature, T_k. Detailed calculations (see, e.g., Danby et al. 1988) show that T_k is an upper limit to T_{ROT}. The expression for T_{ROT} in terms of T_{11}, the peak T_{MB} of the (1, 1) line, and T_{22}, the peak temperature of the (2, 2) line, is (see, e.g., Gaume, Johnston, & Wilson 1992)

$$T_{\mathrm{ROT}} = \frac{41.2}{\ln[3.57(T_{11}/T_{22})]} .$$

For the lower density, lower surface brightness regions, the total column density of NH_3 is assumed to be given by the population of metastable levels only. This population is

$$N_t = N(0, 0) + N(1, 1) + N(2, 2) + N(3, 3) + \cdots .$$

By assuming an LTE population, characterized by a single T_{ROT}, we have

$$N_t = N(1, 1)(\tfrac{1}{3}e^{23/T_{\mathrm{ROT}}} + 1 + \tfrac{5}{3}e^{-41.2/T_{\mathrm{ROT}}} + \tfrac{14}{3}e^{-99.6/T_{\mathrm{ROT}}} + \cdots) = N(1, 1)\Re .$$

For values of T_{ROT} between 15 and 50 K, the value of $\Re$ is between 2.65 and 2.26. The column density of NH_3 molecules in the (1, 1) doublets is given by

$$N(1, 1) = 2.88 \times 10^{13}\Re \int T_{11}\, dV .$$

By applying the Rayleigh-Jeans relation, we can convert from temperature to flux density. Integrating over angle and velocity, for a source at distance D, in kpc, we have for NH_3 inversion lines at 1.3 cm

$$\eta(1, 1) = \int N(1, 1)dA = 6.2\ 10^{13}\Re D^2(\mathrm{kpc})S_{11}(\mathrm{mJy\ km\ s^{-1}}) ,$$

where S_{11} is the sum over the main group of hyperfine components and the source area. Converting the virial mass to total number of H_2 molecules, we obtain X, the relative abundance of NH_3 to H_2, as

$$X = 9.3\ 10^{-11}\frac{\Re D^2(\mathrm{kpc})S_{11}(\mathrm{Jy\ km\ s^{-1}})}{[\Delta V_{1/2}(\mathrm{km\ s^{-1}})]^2 R(\mathrm{pc})} .$$

These results are listed in column (10) of Table 1.

REFERENCES

Alcolea, J., Menten, K. M., Reid, M., & Moran, J. M. 1992, in preparation
Bloemhof, E., Reid, M. J., & Moran, J. M. 1992, ApJ, 397, 500
Danby, G., Flower, D. R., Valiron, P., Schilke, P., & Walmsley, C. M. 1988, MNRAS, 235, 229
Dickel, H. R., & Goss, W. M. 1987, A&A, 185, 271
Dreher, J. W., & Welch, W. J. 1981, ApJ, 245, 891
Elmegreen, B., & Lada, C. J. 1977, ApJ, 214, 725
Gaume, R., Johnston, K. J., & Wilson, T. L. 1992, ApJ, 388, 489
Guilloteau, S., Baudry, A., & Walmsley, C. M. 1985, A&A, 153, 179
Guilloteau, S., Stier, M. T., & Downes, D. 1983, A&A, 126, 10
Harten, R. 1976, A&A, 46, 109
Keto, E. R., Ho, P. T. P., & Reid, M. J. 1987, ApJ, 323, L117
Lada, C. J., Elmegreen, B. G., Cong, H.-I., & Thaddeus, P. 1978, ApJ, 226, L39
Mauersberger, R., Wilson, T. L., & Henkel, C. 1988, A&A, 201, 123
Menten, K. M., Johnston, K. J., Wadiak, E. J., Walmsley, C. M., & Wilson, T. L. 1988, ApJ, 331, L41
Migenes, V., Pauls, T. A., Johnston, K. J., & Wilson, T. L. 1989, ApJ, 347, 294
Norris, R. D., Booth, R. S., & Diamond, P. 1982, MNRAS, 201, 209
Reid, M. J., Myers, P., & Bieging, J. H. 1987, ApJ, 312, 830
Turner, J. L., & Welch, W. J. 1984, ApJ, 287, L81
Wilson, T. L., Bieging, J. H., & Downes, D. 1978, A&A, 63, 1
Wilson, T. L., Johnston, K. J., & Mauersberger, R. M. 1991, A&A, 251, 220
Wilson, T. L., & Mauersberger, R. M. 1990, A&A, 239, 305
Wink, J. E., Mezger, P. G., & Zylka, R. 1988, in NASA CP-3036, ed. A. G. G. Tielens & L. J. Allamandola, 237
Zeng, Q., Hermsen, W., Wilson, T. L., & Batrla, W. 1984, A&A, 140, 160